
Robust Disentanglement of a Few Factors at a Time

Benjamin Estermann*

Institute of Neuroinformatics, ETH Zurich
besterma@ethz.ch

Markus Marks*

Institute of Neuroinformatics, ETH Zurich
marksm@ethz.ch

Mehmet Fatih Yanik

Institute of Neuroinformatics, ETH Zurich
yanik@ethz.ch

Abstract

Disentanglement is at the forefront of unsupervised learning, as disentangled representations of data improve generalization, interpretability, and performance in downstream tasks. Current unsupervised approaches remain inapplicable for real-world datasets since they are highly variable in their performance and fail to reach levels of disentanglement of (semi-)supervised approaches. We introduce population-based training (PBT) for improving consistency in training variational autoencoders (VAEs) and demonstrate the validity of this approach in a supervised setting (PBT-VAE). We then use Unsupervised Disentanglement Ranking (UDR) as an unsupervised heuristic to score models in our PBT-VAE training and show how models trained this way tend to consistently disentangle only a subset of the generative factors. Building on top of this observation we introduce the recursive rPU-VAE approach. We train the model until convergence, remove the learned factors from the dataset and reiterate. In doing so, we can label subsets of the dataset with the learned factors and consecutively use these labels to train one model that fully disentangles the whole dataset. With this approach, we show striking improvement in state-of-the-art unsupervised disentanglement performance and robustness across multiple datasets and metrics.

1 Introduction

Deep Learning has been highly successful in academia as well as industry over the past years, largely in the supervised domain [1]. Unsupervised learning is becoming increasingly important, as for large amounts of datasets human annotation is either limited or not possible and therefore these datasets remain 'unused'. Disentanglement is a sub-field of representation learning that tries to identify the low-dimensional generative factors of high-dimensional data [2]. Higgins et al. [3] introduced the β -VAE, a stricter regularization of a variational auto-encoder (VAE) [4, 5], and showed that this model can find generative factors in the *dsprites* dataset [6] without any supervision. Subsequently, the field of disentanglement expanded quickly, as the potential benefits of finding a disentangled representation of data are plentiful, i.e. they allow for more interpretability, cross-domain transfer, robustness, generalizability across machine learning disciplines, as well as improvement of the performance of downstream tasks, such as classification [7–13]. Locatello et al. [7] showed that fully unsupervised disentanglement might not be possible without any inductive biases. Subsequently, Locatello et al. [14, 15] introduced weak and partial supervision for training disentanglement models to tackle the aforementioned obstacle. There are no labels available for many real-life applications and for some data, generative factors of interest are hard or impossible for humans to annotate.

*contributed equally. Code: https://github.com/besterma/robust_disentanglement

Recently, Duan et al. [8] defined a new, unsupervised heuristic for evaluating the disentanglement performance of models, based on the assumption that models that disentangle well are more likely to be similar to each other than the ones that do not disentangle [16–19]. They demonstrate that this Unsupervised Disentanglement Ranking (UDR) correlates well with metrics that rely on previously annotated labels across various models and datasets [8]. Yet, the problem of extreme hyperparameter sensitivity and therefore a lack of performance and robustness in training disentanglement models remains a major challenge in disentanglement representation learning [7].

This paper introduces a systematic way to train models for disentanglement and increase overall performance and robustness. Our contributions are several-fold:

- We introduce Population Based Training (PBT) [20] for variational training to overcome hyperparameter sensitivity and achieve consistently high performing models.
- We demonstrate PBT-VAE training performance in the supervised and semi-supervised case and show how it can beat the state-of-the-art.
- We extend our approach to unsupervised learning using UDR (PBT-U-VAE (UDR)) and describe how this approach leads to a very consistent disentanglement of the factors with the highest variance in image space.
- We show how these factors can be used to label the dataset, and novel factors can be learned by removing the learned ones from the dataset.
- We demonstrate how these learned labels can be used to train a PBT-VAE and call our approach the recursive PBT-U-VAE (UDR) (rPU-VAE).
- We evaluate how the rPU-VAE disentangles different datasets in comparison to the state-of-the-art.
- We show how the performance of the rPU-VAE depends on the number of labels generated during training.

2 Background and related work

2.1 β -TCVAE

The Variational Autoencoder (VAE) [4, 5] is a widely adapted deep generative model, particularly in state-of-the-art disentanglement approaches. It consists of an encoder network $q(z|x)$ as well as a decoder network $p(x|z)$. It is trained by maximizing the evidence lower bound (ELBO) (Eq. 1 with $\beta=1$). Here $p(z)$ denotes the prior for the latent variables z , which is usually isotropic unit Gaussian. The first ELBO term can be viewed as a negative reconstruction error, while the second term penalizes deviations of the latent code from the prior. Higgins et al. [3] introduced β as a hyperparameter in the (ELBO) of a VAE to increase the weight on the penalization term as follows:

$$L_\beta = \frac{1}{N} \sum_{n=1}^N (\mathbb{E}_q[\log p(x_n|z)] - \beta \text{KL}(q(z|x_n)||p(z))) \quad (1)$$

The authors showed that this loss modification yields increased disentanglement in the representation of data. Chen et al. [21] further decomposed the penalty term $\text{KL}(q(z|x_n)||p(z))$, into an index-code mutual information, a total correlation and a dimension-wise Kullback–Leibler (KL) term:

$$\mathbb{E}_{p(n)}[\text{KL}q(z|n)||p(z))] = \text{KL}(q(z, n)||q(z)p(n)) + \text{KL}(q(z)||\prod_j q(z_j)) + \sum_j \text{KL}(q(z_j)||p(z_j)) \quad (2)$$

where z_j denotes the j th dimension of the latent variable. This formulation of VAE, called β -TCVAE, has been previously shown to perform well on some disentanglement tasks [7]. This is why in this study, we focus on the β -TCVAE as our base model, but in principle, our framework is model agnostic and could therefore be applied to other state-of-the-art models as well.

2.2 Population Based Training

PBT is an optimization algorithm introduced by Jaderberg et al. [20], which can jointly optimize a population of models and their hyperparameters. Compared to grid search or sequential optimization,

PBT results in more stable training, faster learning, and higher performance. It can outperform heavily tuned hyperparameter schedules. Its effectiveness has been shown over different domains, specifically in domains prone to hyperparameter sensitivity, for example, deep reinforcement learning [20]. The algorithm consists of a population \mathcal{P} , with members $\mathcal{M} \in \mathcal{P}$, each member $\mathcal{M} = (\theta, h, p, t)$, where θ are the parameters of the model, h the hyperparameters, p the score, and t the current step. Furthermore, there are the functions $step : \theta \leftarrow step(\theta, h, t)$ and $eval : p \leftarrow eval(\theta)$. Before the training starts, each $\mathcal{M} \in \mathcal{P}$ randomly initializes its weights θ and hyperparameters h . First, each \mathcal{M} gets trained for a certain amount of steps using $step$, and its performance gets evaluated using $eval$. It is important to note that $eval$ does not have to be in any relation with the loss function used during $step$, specifically, it does not need to be differentiable. Next, meta-optimization is performed, where the parameters θ and hyperparameters h are updated given the performance of the entire population. This update is achieved through two functions, which get called independently on each \mathcal{M} : *exploit* allows a member to, given its performance, abandon its solution and focus on a more promising one, *explore* proposes new possible hyperparameters to allow for better exploration of the hyperparameter space. This cycle continues until either the models converge or the computational budget has been exceeded.

2.3 Unsupervised Disentanglement Ranking

Building on top of the probabilistic narrative that disentangled representations are more likely to be similar to each other than entangled ones [16–19], Duan et al. [22] defined a new unsupervised heuristic for disentanglement model selection. More specifically, their approach is based on two main assumptions. First, disentangled representations are, up to permutation and sign inversion, similar to one another, corresponding to a single plausible disentangled generative process. Second, entangled representations are different from one another, as neural networks usually tend to converge to different hidden representations despite being trained on the same task. Therefore, high representational similarity within a set of models indicates a high likelihood of these models being disentangled. To assess a single model’s performance, UDR is computed on a set of models, usually between 5 and 50, with different initial weights but trained using the same hyperparameters. The final score of each model is the median overall pairwise comparison with the other models. Each pairwise comparison is scored according to the similarity of the representations. If this process is repeated over multiple hyperparameters, it is possible to draw conclusions about the fitness of each of these hyperparameter settings and to use that knowledge to guide model selection.

2.4 Disentanglement metrics

Several metrics have been introduced to assess different aspects of disentanglement [3, 21, 23–26]. For a detailed overview, we refer to Supplementary D of [7]. In this study, we focus on MIG [21] and DCI Disentanglement, since it has been demonstrated that for most datasets [7, 15] most of the disentanglement metric correlate. Moreover, the β -VAE metric [3] as well as the FactorVAE [23] require the true underlying generative model and are therefore not suited. Further, the SAP score [26] does not seem to correlate well with the other metrics [15]. MIG enforces each ground truth factor to be learned by a single latent variable, but allows one latent variable to learn, and therefore entangle, multiple ground truth factors. DCI Disentanglement [25] allows us to capture this weakness of MIG, and therefore both metrics give a better picture of disentanglement. Moreover UDR as well as MIG/DCI Disentanglement indicate improvement of the representation with respect to downstream task performance since they are both highly correlated to it [7, 8]. We compute MIG as well as DCI Disentanglement as described in [7] using `disentanglement-lib`¹.

3 (Semi-)supervised PBT-Disentanglement

Locatello et al. [15] introduced a supervision signal in the loss function during training to aid the training process if a limited number of labels are available. They show how models trained in this semi-supervised fashion outperform unsupervised trained models with respect to disentanglement. We show how our approach of training VAEs using PBT (PBT-VAE) can be used to optimize for disentanglement directly during training. We demonstrate how models trained with PBT for disentanglement express very little variance in disentanglement outcome assessed by MIG and DCI

¹https://github.com/google-research/disentanglement_lib

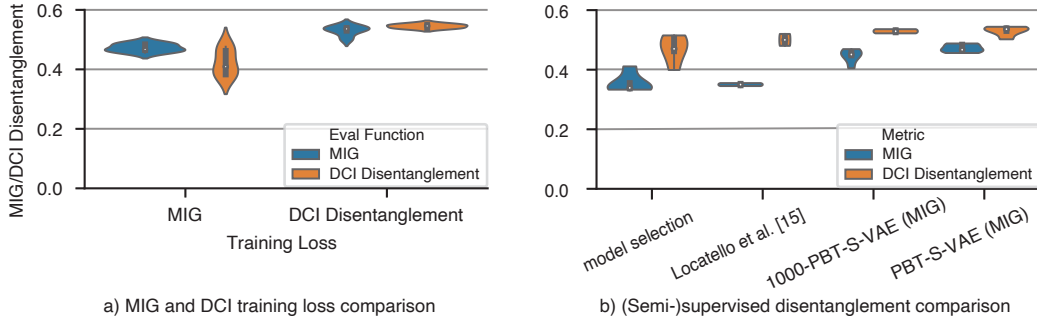


Figure 1: Developing Population Based Training for (semi-)supervised disentanglement. a) MIG is the preferred *eval* function for PBT-S-VAE, as it outperforms DCI Disentanglement when measured with both metrics respectively. b) The semi-supervised 1000-PBT-S-VAE (MIG) outperforms both Locatello et al. [15] and the results of the model selection when all of them are trained on 1000 *dsprites* labels. The fully supervised PBT-S-VAE further increases performance in comparison to the semi-supervised approaches.

Disentanglement, indicating a robust training process. Moreover, with these supervised PBT-VAE disentanglement results, we establish an upper limit for the realistically achievable unsupervised performance in the subsequent chapter. For evaluation of our approaches in this study, we use the *dsprites* [6] and *shapes3d* [27] datasets, as they are some of the most commonly used in the disentanglement literature and therefore enable us to benchmark against other methods [3, 7, 12, 15, 21, 23, 28].

3.1 Comparison of *eval* functions for PBT

PBT-VAE training outcome is contingent on the *eval* function used for PBT. Within our considered metrics of MIG and DCI Disentanglement, we first test what disentanglement each metric used as PBT *eval* function yields, assessed by all other metrics. For each metric, we carry out five separate PBT runs with different random seeds. On *dsprites*, models trained with MIG achieve a higher MIG compared to models trained with DCI Disentanglement, while expressing lower variance (Fig. 1a). Moreover, these models do similarly well, when assessed with DCI Disentanglement compared to models trained with DCI Disentanglement. Based on this experiment, for the rest of the study, we use MIG as *eval* function and call the approach PBT-S-VAE (MIG). Generally, this approach is not limited to either MIG or DCI Disentanglement as an *eval* function and more functions can be assessed in the future for a variety of datasets.

3.2 (Semi-)supervised PBT performance

Locatello et al. [15] demonstrated increased disentanglement over the unsupervised baseline using a few-label approach, a realistic alternative to fully supervised approaches for practical applications. We include this approach as a semi-supervised baseline for later comparison. As another baseline, we use the performance of simple model selection. After the finishing training of a set of models, we selected the best model based on their MIG calculated on 1000 randomly selected labels. Finally, we introduce our semi-supervised and fully supervised PBT based approaches. The **semi-supervised** 1000-PBT-S-VAE (MIG) had access a randomly sub-sampled set of 1000 labels, similar to [15] and the model selection baseline, whereas the **supervised** PBT-S-VAE (MIG) was trained using the complete set of labels. All models were trained on the *dsprites* dataset. We see that 1000-PBT-S-VAE (MIG) outperforms both baselines clearly in terms of mean MIG and DCI Disentanglement scores, only surpassed by the PBT-S-VAE (MIG), while showing reduced variance (Fig. 1b).

4 Unsupervised PBT-Disentanglement

We now extend our approach to the unsupervised setting after having established the use of PBT for VAE disentanglement training. We use UDR [8] as an unsupervised *eval* function instead of the MIG in the PBT framework, which allows us to move our PBT-S-VAE (MIG) approach towards being an

unsupervised method (PBT-U-VAE). We adapt our PBT-VAE approach to fulfill the assumptions of the UDR, namely for PBT-U-VAE (UDR), each $\mathcal{M} \in \mathcal{P}$ consists of five models separately initialized and trained with the same hyperparameters h . We denote the weights of all five models as θ . According to Duan et al. [8], five models provide a reasonable estimate of disentanglement, while allowing the approach to be computationally feasible.

4.1 Consistent disentanglement of factors with the largest variation

We found that using PBT-U-VAE (UDR), the well-performing models disentangled only ground truth factors with high variance in image space (Fig. 2). While these models did not capture the whole variation in image space, they still achieved high UDR scores and consistently learned the same factors. Once they reached that representation, they failed to capture any new factors of variation during further training epochs. Therefore, the resulting MIG/DCI Disentanglement scores displayed in Fig. 2 are relatively low. This behavior could be accounted for by the fact that the UDR does not consider the number of active latent variables, so a group of models capturing all ground truth factors cannot achieve a better UDR score than models capturing only a distinct subset of those factors.

4.2 Recursive PBT-U-VAE (UDR)

We shortly summarize the assumptions we can make given the previous findings:

- PBT-U-VAE (UDR) yields consistent disentangling of a subset of factors.
- PBT-U-VAE (UDR) training converges after these factors have been learned.
- Models, which disentangle those factors, fail to learn any new factors of variation.

These assumptions allow us to design our recursive PBT-U-VAE (UDR) algorithm, overcoming the limitations of the vanilla PBT-U-VAE (UDR) approach. We try to recursively remove variation of learned active latent variables from the input dataset. With this reduced dataset, we start another round of PBT-U-VAE (UDR) training, forcing the network to learn new factors of variation. Algorithm 1 shows the implementation of this approach in pseudo-code. For a graphical summary, please see Fig. 7 in the Supplementary A.

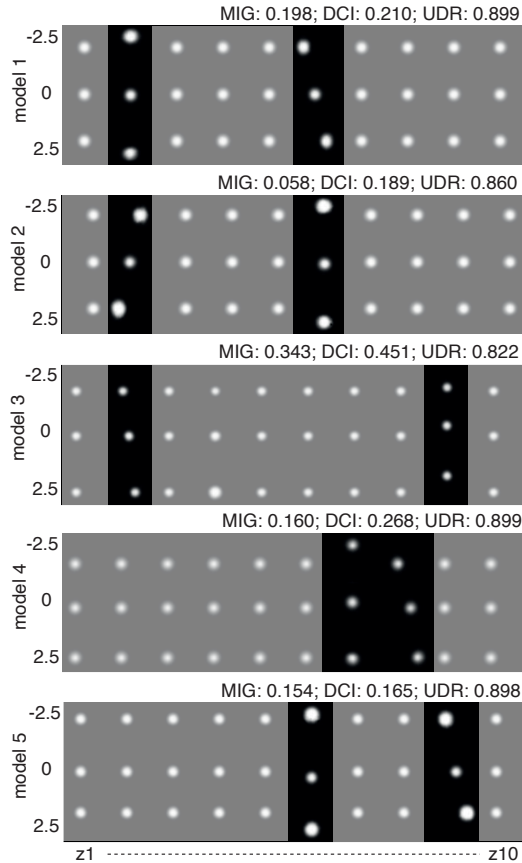


Figure 2: For 5 different random seeds on *dsprites*, PBT-U-VAE (UDR) models consistently disentangle x and y position while reaching high UDR scores. VAE latent variables are indicated with z_1, \dots, z_{10} and active latent variables z_{active} are highlighted by increased contrast.

Algorithm 1 recursive PBT-U-VAE (UDR)(rPU-VAE)

```
1: procedure DISENTANGLE( $\mathcal{D}$ ) ▷ initial dataset  $\mathcal{D}$ 
2:    $surrogateLabels \leftarrow emptyList()$ 
3:    $labels_0 \leftarrow$  PBT-U-VAE (UDR) ( $\mathcal{D}$ ) ▷ Train until convergence
4:    $surrogateLabels.append(labels_0)$ 
5:   for  $i \leftarrow 1, MaxNrLeafRuns$  do ▷ Start leaf-runs
6:      $leafLabels \leftarrow emptyList()$ 
7:      $d \leftarrow reduce(\mathcal{D}, labels_0, i)$  ▷ Remove variance of the labeled factor
8:     while  $|d| > size_{d-min} \wedge$  no convergence do ▷ Recursively label and reduce dataset
9:        $labels_i \leftarrow$  PBT-U-VAE (UDR) ( $d$ ) ▷ This is one metaEpoch
10:       $leafLabels.append(labels_i)$ 
11:       $d \leftarrow reduce(d, labels_i, 0)$ 
12:    end while
13:     $surrogateLabels.append(leafLabels)$ 
14:  end for
15:   $\theta \leftarrow$  PBT-S-VAE (MIG) ( $\mathcal{D}, surrogateLabels$ ) ▷ Train final model
16:  return  $\theta$ 
17: end procedure
```

Initial PBT training until first convergence. We start with the initial dataset and train our PBT-U-VAE (UDR) approach until the change of UDR score of the best $\mathcal{M} \in \mathcal{P}$ is below a predefined threshold ($\Delta UDR < threshold_{UDR}$) for a fixed number of epochs. If this criterion is reached, we consider this first metaEpoch to be finished. This member \mathcal{M} has now learned a subset of the ground-truth factors.

Removal of variation explained by learned active latents. To remove learned factors, we select the best VAE from the set of VAEs of the best member $\mathcal{M} \in \mathcal{P}$. We identify the most active latent variables z of this model by their respective KL divergence to the prior, if $KL(q(z_a|x)||p(z_a)) > threshold_{z_{active}}$, z_a is active, otherwise not, following the argumentation of [8, 19]. We try to reduce the dataset, such that the variance that can be explained by these z_{active} is minimized. To do so, we map the whole dataset onto z_{active} using the encoder $q(z|x)$ of the earlier selected VAE. We use the resulting latent encoding values (LEV) as labels of the dataset, which we refer to as surrogate labels subsequently. Next, we calculate the derivative over the sorted surrogate labels to determine intervals of the dataset over which the selected factors change least (Fig. 3), while trying to keep the resulting dataset as large as possible. To find such intervals, we compute the ratio between the lower of the two adjacent peaks and the mean within the interval.

This ratio allows us to identify intervals which best suit the above mentioned criteria. If multiple active latent variables z_{active} were learned, we intersect the intervals of these factors to get a subset of the dataset where all of these factors vary least. In other words, this is a set intersection of the sets of all elements in the current dataset where the respective latent gets mapped onto an interval of least variation. This reduced dataset will be used for the next metaEpoch of PBT-U-VAE (UDR) training. Having removed most of the variation of the

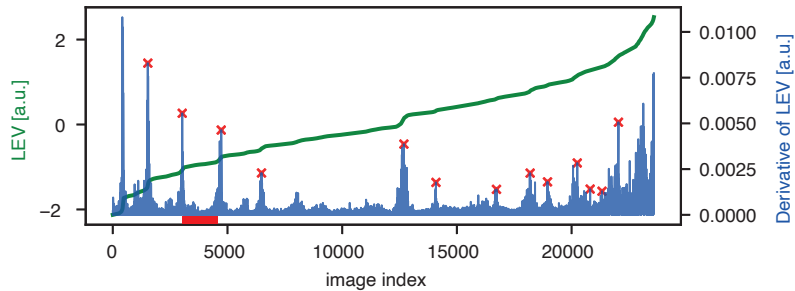


Figure 3: Illustration of the latent encoding and data reduction approach. After one metaEpoch, the best VAE from the population is used to encode the whole *dsprites* dataset onto an z_{active} . The data is sorted by their encoding values (green line), and the derivative is computed (blue line). Subsequently, we calculate peaks in the derivatives (red crosses) and select an interval in between the peaks in which the latent variable is not highly variable (red horizontal bar).

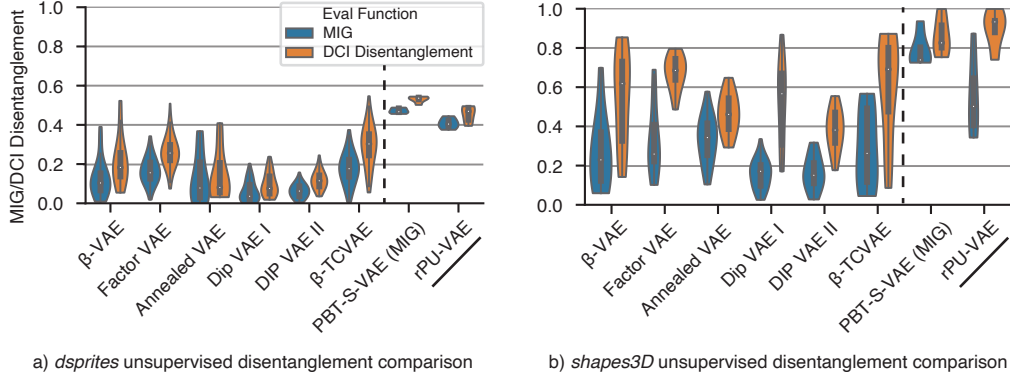


Figure 4: rPU-VAE outperforms previous approaches on commonly used benchmarks. a) comparison of rPU-VAE performance to unsupervised state-of-the-art approaches [3, 21, 23, 26, 28]. The rPU-VAE beats all previous models with respect to mean MIG/DCI Disentanglement scores and has comparatively little variance. It almost reaches disentanglement scores of our supervised PBT-S-VAE (MIG), which we introduced as an upper limit for the performance. b) Same comparison as in a), but on the *shapes3d* dataset. rPU-VAE again outperforms the state-of-the-art and performs very close to our PBT-S-VAE (MIG).

learned latent variables from the dataset forces the network to learn new factors of variation if they exist.

Leaf-run. After some number of metaEpochs and subsequent dataset reduction, all the variance is removed from the dataset and the models only learn noise and fail to reach a certain UDR score $\forall_{M \in \mathcal{P}} eval(\theta(M)) < UDR_{threshold}$. Alternatively, we also stop training when the reduced dataset becomes too small ($|d| < size_{d-min}$). One such path of recursive metaEpochs we consider as a leaf-run. During each leaf-run, a subset of the original dataset gets surrogate labels assigned, increasing the number of leaf-runs, therefore, increases the amount of total surrogate labels. We could recursively generate a tree from all z_{active} intervals, where the height of the tree is the number of all learned factors, given that the dataset includes all possible combinations of ground truth factors.

Combining all learned factors into a single model. With this recursive application of PBT-U-VAE (UDR) and dataset reduction, we can identify most factors of variation of a data distribution and, at the same time, label parts of the data. Subsequently, we use this partially annotated dataset as a supervision signal for the previously mentioned PBT-S-VAE (MIG). The resulting model from PBT-S-VAE (MIG) now captures all of the previously discovered factors at the same time. We name the whole algorithm the recursive PBT-U-VAE (UDR) or rPU-VAE.

5 Experiments on unsupervised disentanglement

We demonstrate quantitatively that the rPU-VAE achieves consistently higher scores than state-of-the-art approaches across multiple datasets and metrics while being more robust. We compare the performance of our rPU-VAE approach to the unsupervised β -TCVAE [21], β -VAE [3], FactorVAE [23], DIP-VAE-I and DIP-VAE-II [26] and AnnealedVAE [28], where pretrained models are partially available from [7] as part of `disentanglement-lib`. Each of these models was trained with 50 random seeds and a range of hyperparameters, specified in Supplementary E in [7]. Since *shapes3d* models are not publicly available on `disentanglement-lib` we recomputed that data according to [7].

We train our rPU-VAE approach with 5 random seeds and 3 leaf-runs. We note that the rPU-VAE achieves significantly higher mean disentanglement scores for all datasets used in Fig. 4. As expected, the robustness of disentanglement is higher (see the drastically reduced variance compared to other approaches). The unsupervised rPU-VAE MIG/DCI Disentanglement scores are very close to our previously introduced supervised PBT-S-VAE (MIG) model. Noticeably, the MIG for *shapes3d* still has a larger gap to the supervised upper-bound when compared to *dsprites*. Models learn color-related ground truth factors with multiple active latent variables, which decreases the MIG for *shapes3d*.

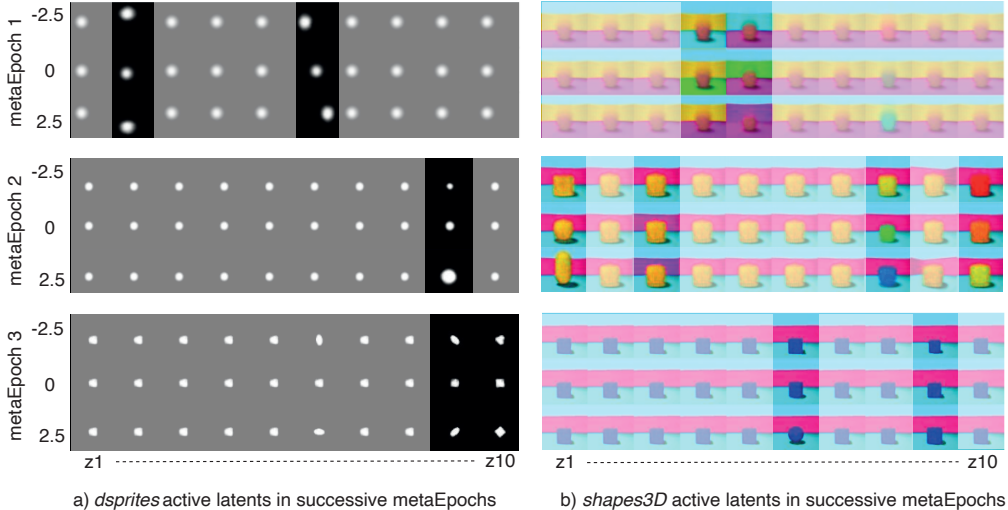


Figure 5: Representative examples of latent traversals at each of 3 metaEpochs during rPU-VAE training. VAE latent variables are indicated with z_1, \dots, z_{10} and active latent variables z_{active} are highlighted by increased contrast. a) Traversals of *dsprites* dataset. metaEpoch 1: z_{active} encode y and x position; metaEpoch 2: z_{active} code for scale; metaEpoch 3: z_{active} code for rotation and shape. b) Traversals of *shapes3d* dataset. metaEpoch 1: z_{active} code for wall and floor colors; metaEpoch 2: z_{active} code for shape, wall color and twice color of the object; metaEpoch 3: z_{active} code for shape of the object and scale.

Nevertheless, we argue that this representation of color is valid and, in fact, disentangled, as each latent variable only represents (parts of) a single ground truth factor, as would one when expressing color using the RGB color model. Looking at what the models learn with each metaEpoch (Fig. 5), we can see that at each metaEpoch distinct generative factors are learned. We provide more detail on how hyperparameters developed during learning in Supplementary section B while defining all hyperparameters used in Supplementary section E. We show representative full traversals for *shapes3d* in Fig. 12. Moreover, we present full traversals of our models trained on *celebA* [29] and demonstrate the capability of rPU-VAE to find interesting and non-trivial factors in this naturalistic dataset in Fig. 13. Lastly, we include full traversals of the final model on *dsprites* in Fig. 14b. While during leaf-runs, our models managed to capture factors such as shape and rotation (Fig. 5a), the final model learns only scale, x-position and y-position. We note that this is the same for the supervised model PBT-S-VAE (Fig. 14a).

5.1 Amount of labels needed

As mentioned in Section 4.2, we could potentially aim to label the whole dataset in order to use these surrogate labels for training the rPU-VAE, but this would be computationally expensive. We showed in Section 3.2 that disentangling models can be successfully trained with a fraction of the ground-truth labels, so we assume that this holds for our surrogate labels as well. We test how the number of leaf-runs in rPU-VAE training affects MIG/DCI Disentanglement

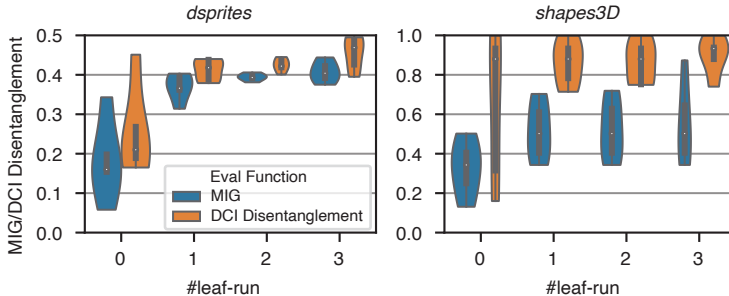


Figure 6: Performance of rPU-VAE with respect to number of leaf-runs. For *dsprites* and *shapes3d* MIG/DCI Disentanglement improve with the number of leaf-runs, particularly from leaf-run 0 to leaf-run 1.

performance on *shapes3d* as well as *dsprites*, using 1-3 leaf-runs during training for each of the 5 models (Fig. 6). For the *shapes3d* and *dsprites* dataset the performance of rPU-VAE improves over both metrics with the number of leaf-runs. We observe the biggest improvement from performing 0 to performing 1 leaf-run. Not only does the overall performance improve with leaf-runs, but also the variance of the MIG/DCI Disentanglement scores tends to reduce with each leaf-run.

6 Conclusions

We motivate the rPU-VAE, a new approach for consistent unsupervised disentanglement. We evaluate our approach across multiple datasets and disentanglement metrics against state-of-the-art approaches. The results show the superior performance of rPU-VAE compared to previously used models, not only in terms of improved average performance but also in terms of drastically reduced variance. We experiment with how the number of recursions within the rPU-VAE training affects disentanglement performance. We show how PBT can be used for achieving an increased performance in the semi-supervised setting as well. Finally, we show qualitative results of our method applied to the naturalistic dataset *celebA*. Particularly because of the enhanced robustness, our approach is one step closer to enabling practitioners to leverage the benefits of disentangled representations of their data without the need for annotation.

7 Broader Impact

Robust disentangled representations are directly applicable to many domains within science and medicine. In recent years, many unsupervised methods, i.e. dimensionality reduction and manifold techniques, have been used to discover structure in complex datasets in physics [30], genomics [31, 32], neuroscience [33] and energy prediction [34]. Not only do these provide an opportunity in discovering underlying structure in natural phenomena, but also human biases can be reduced by data-driven analysis.

Similarly, there has been a surge in use of unsupervised learning in medicine such as drug design [35], detection of brain lesions [36], cardiac image analysis [37] and drug side effect discovery [38]. Unsupervised approaches have been also highly successful in experimental Brain-Machine-Interfaces (BMI) [39], leading to higher stability of BMI readouts.

However, the enhanced interpretability of disentangled representations in these applications might lead to undue sense of trust and greater negative consequences in case of failures. Thus, further research on reliability of AI approaches has to be done beyond the proof-of-principle.

Our algorithm relies on training large numbers of models, requiring significant computational resources. Therefore energy consumption and resulting CO₂ footprint can be quite substantial [40]. The aforementioned benefits of utilizing disentangled representations to improve outcomes in science and medicine are difficult to weigh against the entailing environmental costs and need to be evaluated on a case-by-case basis. Alternatively, further research (such as use of spiking neural networks [41]) may make our approach much more computationally efficient.

8 Acknowledgments and Disclosure of Funding

We thank Francesco Locatello for helping us to re-use `disentanglement-lib` and for fruitful discussions. We thank Hafsteinn Einarsson for the very useful feedback on the manuscript.

This project was funded by the Swiss Federal Institute of Technology (ETH) Zurich and the European Research Council (ERC) under the European Union’s Horizon 2020 research and innovation program (grant agreement No 818179).

The authors declare no conflicts of interests.

References

- [1] Ian Goodfellow, Yoshua Bengio, and Aaron Courville. *Deep Learning*. MIT Press, 2016. <http://www.deeplearningbook.org>.
- [2] Yoshua Bengio, Aaron Courville, and Pascal Vincent. Representation learning: A review and new perspectives. *IEEE transactions on pattern analysis and machine intelligence*, 35(8): 1798–1828, 2013.
- [3] Irina Higgins, Loic Matthey, Xavier Glorot, Arka Pal, Benigno Uria, Charles Blundell, Shakir Mohamed, and Alexander Lerchner. Early visual concept learning with unsupervised deep learning. *arXiv preprint arXiv:1606.05579*, 2016.
- [4] Diederik P Kingma and Max Welling. Auto-encoding variational bayes. *arXiv preprint arXiv:1312.6114*, 2013.
- [5] Danilo Jimenez Rezende, Shakir Mohamed, and Daan Wierstra. Stochastic backpropagation and approximate inference in deep generative models. *arXiv preprint arXiv:1401.4082*, 2014.
- [6] Loic Matthey, Irina Higgins, Demis Hassabis, and Alexander Lerchner. dsprites: Disentanglement testing sprites dataset. <https://github.com/deepmind/dsprites-dataset/>, 2017.
- [7] Francesco Locatello, Stefan Bauer, Mario Lucic, Gunnar Rätsch, Sylvain Gelly, Bernhard Schölkopf, and Olivier Bachem. Challenging common assumptions in the unsupervised learning of disentangled representations. *arXiv preprint arXiv:1811.12359*, 2018.
- [8] Sunny Duan, Nicholas Watters, Loic Matthey, Christopher P Burgess, Alexander Lerchner, and Irina Higgins. A heuristic for unsupervised model selection for variational disentangled representation learning. *arXiv preprint arXiv:1905.12614*, 2019.

- [9] Alexander A Alemi, Ian Fischer, Joshua V Dillon, and Kevin Murphy. Deep variational information bottleneck. *arXiv preprint arXiv:1612.00410*, 2016.
- [10] Francesco Locatello, Gabriele Abbati, Thomas Rainforth, Stefan Bauer, Bernhard Schölkopf, and Olivier Bachem. On the fairness of disentangled representations. In *Advances in Neural Information Processing Systems*, pages 14584–14597, 2019.
- [11] Christopher Grimm, Irina Higgins, Andre Barreto, Denis Teplyashin, Markus Wulfmeier, Tim Hertweck, Raia Hadsell, and Satinder Singh. Disentangled cumulants help successor representations transfer to new tasks. *arXiv preprint arXiv:1911.10866*, 2019.
- [12] Sjoerd van Steenkiste, Francesco Locatello, Jürgen Schmidhuber, and Olivier Bachem. Are disentangled representations helpful for abstract visual reasoning? In *Advances in Neural Information Processing Systems*, pages 14222–14235, 2019.
- [13] Abel Gonzalez-Garcia, Joost Van De Weijer, and Yoshua Bengio. Image-to-image translation for cross-domain disentanglement. In *Advances in neural information processing systems*, pages 1287–1298, 2018.
- [14] Francesco Locatello, Ben Poole, Gunnar Rätsch, Bernhard Schölkopf, Olivier Bachem, and Michael Tschannen. Weakly-supervised disentanglement without compromises. *arXiv preprint arXiv:2002.02886*, 2020.
- [15] Francesco Locatello, Michael Tschannen, Stefan Bauer, Gunnar Rätsch, Bernhard Schölkopf, and Olivier Bachem. Disentangling factors of variation using few labels. *arXiv preprint arXiv:1905.01258*, 2019.
- [16] Yixuan Li, Jason Yosinski, Jeff Clune, Hod Lipson, and John E Hopcroft. Convergent learning: Do different neural networks learn the same representations? In *FE@NIPS*, 2015.
- [17] Ari Morcos, Maithra Raghu, and Samy Bengio. Insights on representational similarity in neural networks with canonical correlation. In *Advances in Neural Information Processing Systems*, pages 5727–5736, 2018.
- [18] Liwei Wang, Lunjia Hu, Jiayuan Gu, Zhiqiang Hu, Yue Wu, Kun He, and John Hopcroft. Towards understanding learning representations: To what extent do different neural networks learn the same representation. In *Advances in Neural Information Processing Systems*, pages 9584–9593, 2018.
- [19] Michal Rolínek, Dominik Zietlow, and Georg Martius. Variational autoencoders pursue pca directions (by accident). In *Proceedings of the IEEE Conference on Computer Vision and Pattern Recognition*, pages 12406–12415, 2019.
- [20] Max Jaderberg, Valentin Dalibard, Simon Osindero, Wojciech M Czarnecki, Jeff Donahue, Ali Razavi, Oriol Vinyals, Tim Green, Iain Dunning, Karen Simonyan, et al. Population based training of neural networks. *arXiv preprint arXiv:1711.09846*, 2017.
- [21] Tian Qi Chen, Xuechen Li, Roger B Grosse, and David K Duvenaud. Isolating sources of disentanglement in variational autoencoders. In *Advances in Neural Information Processing Systems*, pages 2610–2620, 2018.
- [22] Irina Higgins, David Amos, David Pfau, Sebastien Racaniere, Loic Matthey, Danilo Rezende, and Alexander Lerchner. Towards a definition of disentangled representations. *arXiv preprint arXiv:1812.02230*, 2018.
- [23] Hyunjik Kim and Andriy Mnih. Disentangling by factorising. *arXiv preprint arXiv:1802.05983*, 2018.
- [24] Karl Ridgeway and Michael C Mozer. Learning deep disentangled embeddings with the f-statistic loss. In *Advances in Neural Information Processing Systems*, pages 185–194, 2018.
- [25] Cian Eastwood and Christopher KI Williams. A framework for the quantitative evaluation of disentangled representations. *International Conference on Learning Representations*, 2018.
- [26] Abhishek Kumar, Prasanna Sattigeri, and Avinash Balakrishnan. Variational inference of disentangled latent concepts from unlabeled observations. *arXiv preprint arXiv:1711.00848*, 2017.
- [27] Chris Burgess and Hyunjik Kim. 3d shapes dataset. <https://github.com/deepmind/3dshapes-dataset/>, 2018.

- [28] Christopher P Burgess, Irina Higgins, Arka Pal, Loic Matthey, Nick Watters, Guillaume Desjardins, and Alexander Lerchner. Understanding disentangling in β -vae. *arXiv preprint arXiv:1804.03599*, 2018.
- [29] Ziwei Liu, Ping Luo, Xiaogang Wang, and Xiaoou Tang. Large-scale celebfaces attributes (celeba) dataset. *Retrieved August*, 2018.
- [30] Andrea Rocchetto, Edward Grant, Sergii Strelchuk, Giuseppe Carleo, and Simone Severini. Learning hard quantum distributions with variational autoencoders. *npj Quantum Information*, 4(1):1–7, 2018.
- [31] Jiarui Ding, Anne Condon, and Sohrab P Shah. Interpretable dimensionality reduction of single cell transcriptome data with deep generative models. *Nature communications*, 9(1):1–13, 2018.
- [32] Etienne Becht, Leland McInnes, John Healy, Charles-Antoine Dutertre, Immanuel WH Kwok, Lai Guan Ng, Florent Ginhoux, and Evan W Newell. Dimensionality reduction for visualizing single-cell data using umap. *Nature biotechnology*, 37(1):38, 2019.
- [33] Alexander B Wiltschko, Matthew J Johnson, Giuliano Iurilli, Ralph E Peterson, Jesse M Katon, Stan L Pashkovski, Victoria E Abaira, Ryan P Adams, and Sandeep Robert Datta. Mapping sub-second structure in mouse behavior. *Neuron*, 88(6):1121–1135, 2015.
- [34] Elena Mocanu, Phuong H Nguyen, Wil L Kling, and Madeleine Gibescu. Unsupervised energy prediction in a smart grid context using reinforcement cross-building transfer learning. *Energy and Buildings*, 116:646–655, 2016.
- [35] Rafael Gómez-Bombarelli, Jennifer N Wei, David Duvenaud, José Miguel Hernández-Lobato, Benjamín Sánchez-Lengeling, Dennis Sheberla, Jorge Aguilera-Iparraguirre, Timothy D Hirzel, Ryan P Adams, and Alán Aspuru-Guzik. Automatic chemical design using a data-driven continuous representation of molecules. *ACS central science*, 4(2):268–276, 2018.
- [36] Xiaoran Chen and Ender Konukoglu. Unsupervised detection of lesions in brain mri using constrained adversarial auto-encoders. *arXiv preprint arXiv:1806.04972*, 2018.
- [37] Carlo Biffi, Ozan Oktay, Giacomo Tarroni, Wenjia Bai, Antonio De Marvao, Georgia Doumou, Martin Rajchl, Reem Bedair, Sanjay Prasad, Stuart Cook, et al. Learning interpretable anatomical features through deep generative models: Application to cardiac remodeling. In *International Conference on Medical Image Computing and Computer-Assisted Intervention*, pages 464–471. Springer, 2018.
- [38] Fenglong Ma, Chuishi Meng, Houping Xiao, Qi Li, Jing Gao, Lu Su, and Aidong Zhang. Unsupervised discovery of drug side-effects from heterogeneous data sources. In *Proceedings of the 23rd ACM SIGKDD International Conference on Knowledge Discovery and Data Mining*, pages 967–976, 2017.
- [39] Chethan Pandarinath, Daniel J O’Shea, Jasmine Collins, Rafal Jozefowicz, Sergey D Stavisky, Jonathan C Kao, Eric M Trautmann, Matthew T Kaufman, Stephen I Ryu, Leigh R Hochberg, et al. Inferring single-trial neural population dynamics using sequential auto-encoders. *Nature methods*, 15(10):805–815, 2018.
- [40] Emma Strubell, Ananya Ganesh, and Andrew McCallum. Energy and policy considerations for deep learning in nlp. *arXiv preprint arXiv:1906.02243*, 2019.
- [41] Michael Pfeiffer and Thomas Pfeil. Deep learning with spiking neurons: opportunities and challenges. *Frontiers in neuroscience*, 12:774, 2018.

A rPU-VAE Concept Illustration

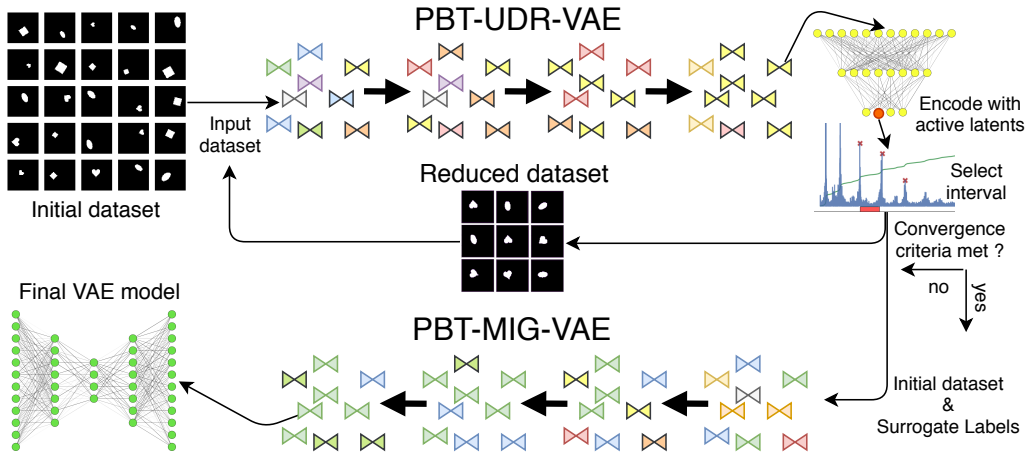


Figure 7: Illustration of the rPU-VAE workflow. The initial dataset is used for training a population of UDR-VAE models. After convergence, the best UDR-VAE of the population is selected and an active latent (red unit in yellow VAE encoder) is determined, and the dataset is encoded. Afterwards, labels are sorted, their derivative calculated and a candidate interval selected (red horizontal bar). The dataset is reduced to this interval and PBT-U-VAE (UDR) training is started again. In leaf-runs, parts of the dataset are annotated with surrogate labels. After a convergence criterion is met, the surrogate labels are then used to train a PBT-S-VAE (MIG), yielding a fully disentangling VAE.

B PBT Training Details

We present the evolution of hyperparameters during population based training. While during supervised PBT-S-VAE training the learning rate remains relatively stable across epochs, the batch size tends to increase over time (Fig. 8a,b). Moreover, we see that our training automatically discovers to anneal β during training. We show the increase of average populations scores over epochs on supervised PBT-S-VAE runs (Fig. 9) as well as the unsupervised PBT-U-VAE leaf-runs (Fig. 10). The hyperparameter schedules during unsupervised PBT-U-VAE leaf-runs appear to be much more non-linear (Fig. 11). In this case the learning rate increases over epochs, while the batch size decreases. β also seems to anneal overall, but with much stronger fluctuations, particularly in epoch 0.

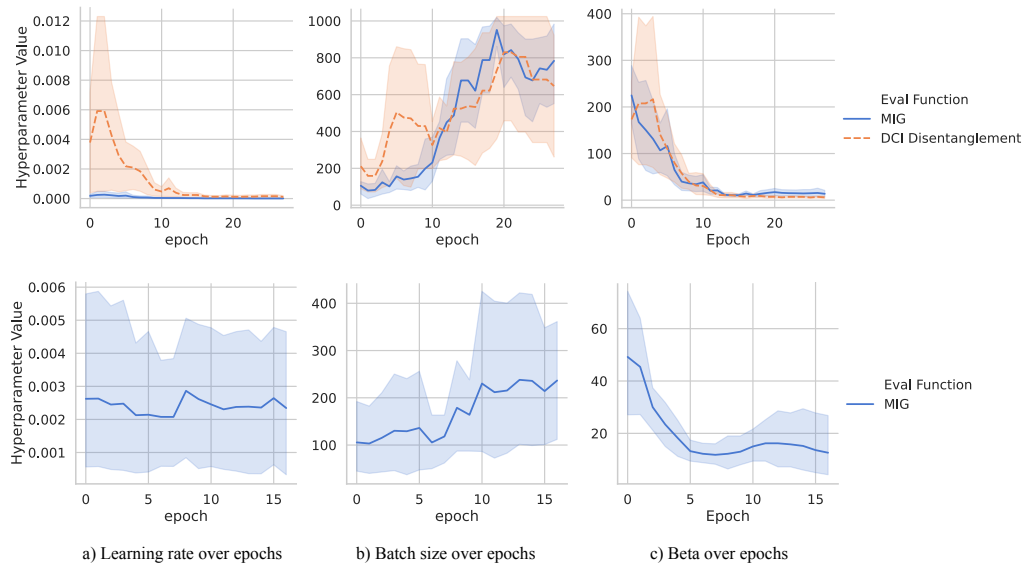


Figure 8: PBT uses dynamic training schedules during supervised training runs on the *dsprites* (top) as well as *shap3d* (bottom) datasets. Displayed are the hyperparameters of the final best-performing model of each PBT run. It discovers annealing of β over epochs (c) for both datasets. In case of *dsprites*, all trainings exhibit a decaying learning rate schedule (a), even though for MIG based training, the learning rate is substantially lower in general. Interestingly when training with DCI, the learning rate increases first before decaying. Batch size (b) has a clear upward trend toward the latter half of training and seems to trend opposite to the annealing β (c).

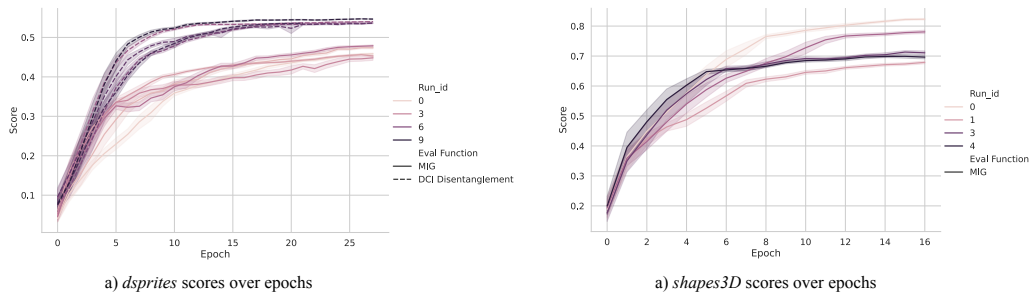


Figure 9: Average population score development during supervised PBT based training. During *dsprites* training (a), DCI based runs start to plateau after 10 epochs, while MIG scores runs are still improving after 26 epochs, indicating they could benefit from longer training. For *shap3d* training, models start to converge after the 10th epoch.

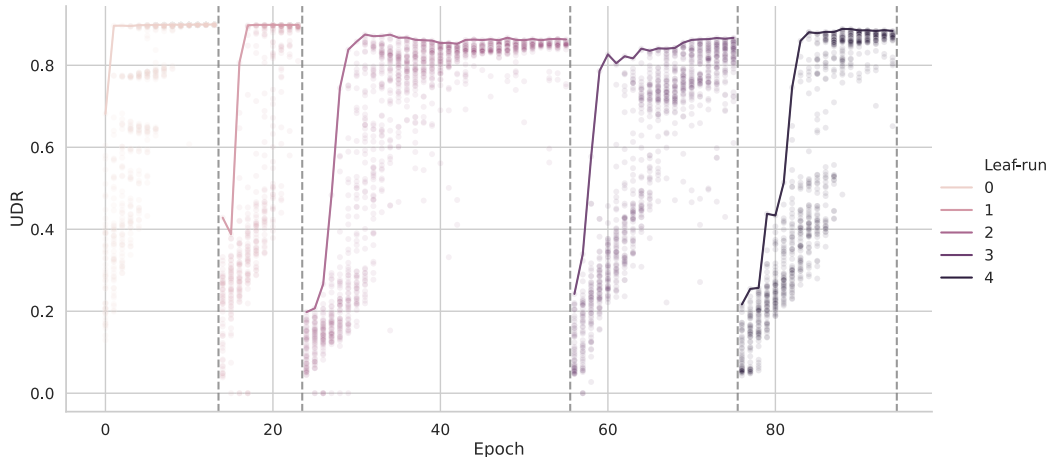


Figure 10: UDR development during rPU-VAE training on *dsprites*. From left to right recursive leaf-runs 0 to 4 are depicted. Each score of a model of the population is shown as a circle and the maximum UDR of the population as a solid line. The later leaf-runs take longer to converge, since the data for training is becoming smaller and noisier with each leaf-run.

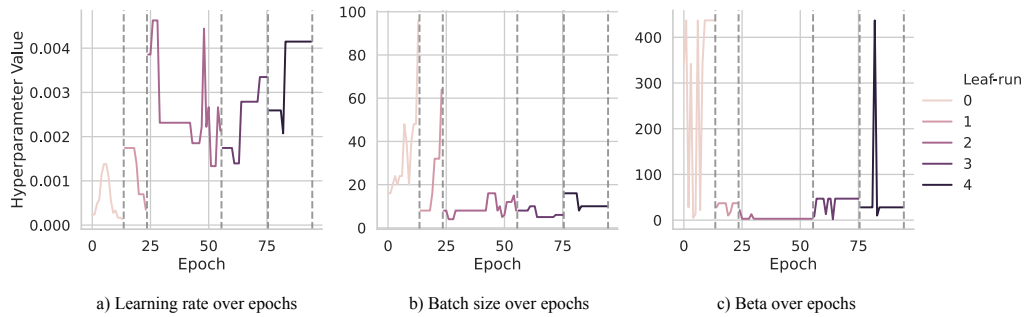


Figure 11: Hyperparameter schedules during leaf-runs on *dsprites*. a) There is a trend of learning rate increase with each leaf-run. b) Contrary to the PBT-S-VAE runs, the batch size stays relatively small, since also the dataset size is decreased with each leaf-run. c) After the first leaf-run, β is drastically decreased and stays relatively low (except a couple of spikes) during subsequent leaf-runs.

C Visualization of Full Traversals

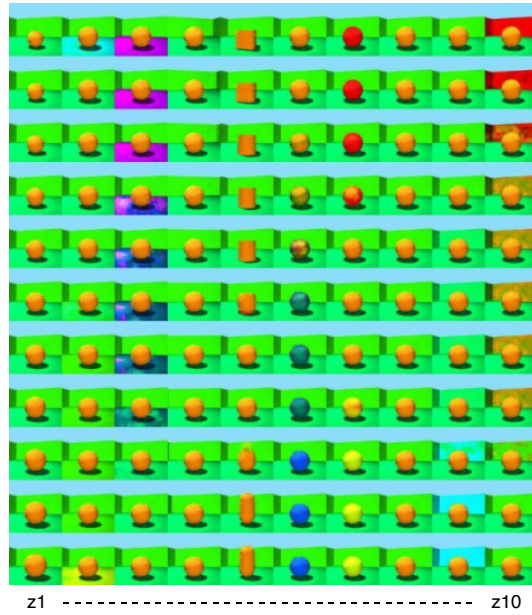


Figure 12: Full traversal of a representative rPU-VAE model trained on *shapes3d*. Latent representations (from left to right): object scale, floor color, floor color, view angle, object shape, object color, object color, inactive, wall color, wall color.

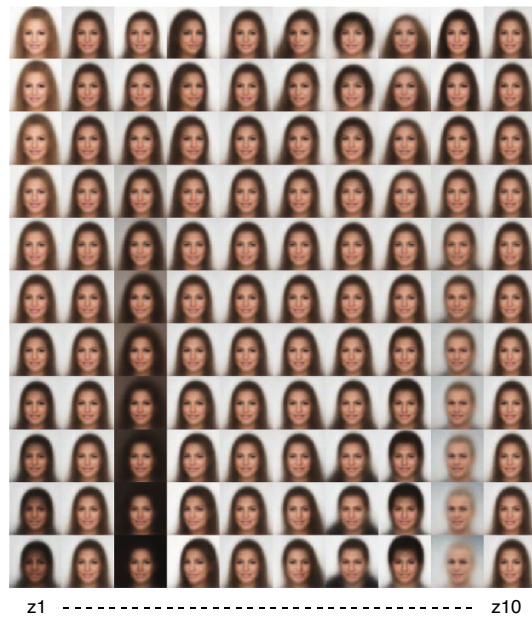


Figure 13: Full traversal of a representative rPU-VAE model trained on *celeba*. Latent representations (from left to right): skin color, inactive, background color, head rotation, inactive, hair orientation, haircut, bangs, baldness, inactive.

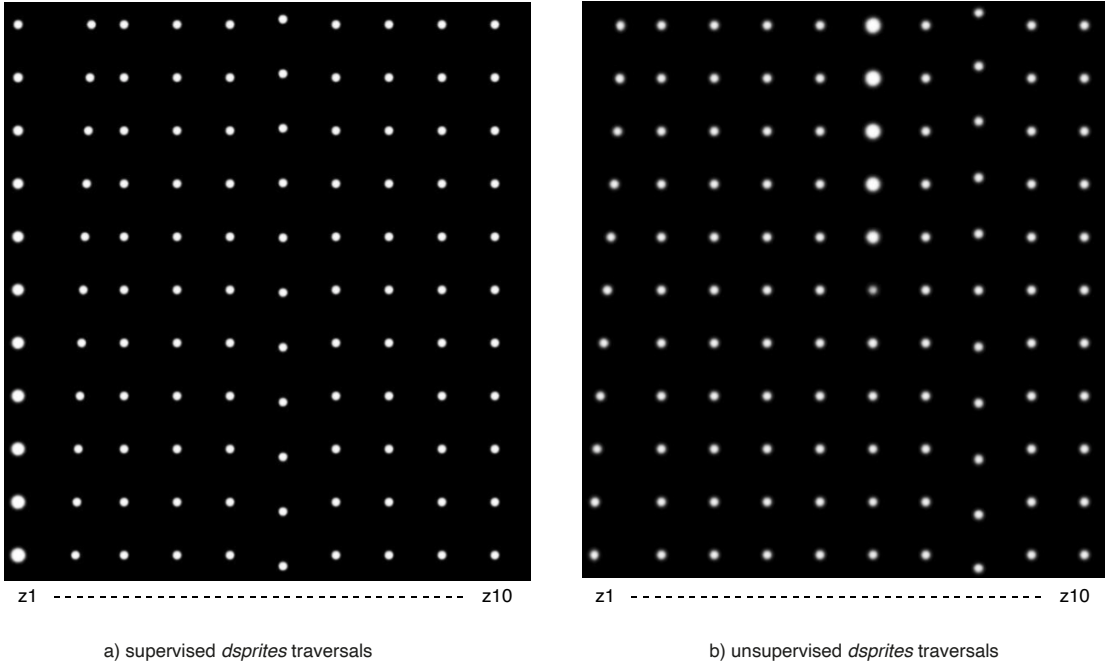


Figure 14: Full traversal of a representative models trained on *dsprites*. a) For comparison to the following unsupervised model, we present traversals of supervised model PBT-S-VAE trained on *dsprites*, interestingly only scale ($z1$), x-position($z2$) and y-position are learned ($z6$). a) Traversals of a representative rPU-VAE model trained on *dsprites*. Again, only scale ($z6$), x-position($z1$) and y-position are learned ($z8$).

D Datasets

Dataset	Ground Truth Factors
Dsprites	32xXposition, 32xYposition, 6xScale, 40xRotation, 3xShape
Shapes3D	10xFloorColor, 10xWallColor, 10xObjectColor, 8xObjectSize, 4xObjectType, 15xAzimuth
CelebA	Shadow, Arch. Eyebrows, Attractive, Bags un. Eyes, Bald, Bangs, Big Lips, Big Nose, Black Hair, Blond Hair, Blurry, Brown Hair, Bushy Eyebrows, Chubby, Eyeglasses, Goatee, Gray Hair, Heavy Makeup, High Cheekbones, Male

Table 1: Summary of Ground Truth Factors for the *dsprites*, *shapes3d* and *celebA* datasets

E Hyperparameters

E.1 Architecture and Parameters of β -TCVAE

Encoder	Decoder
Input: [64,64,num channels]	FC, 256 ReLU
4x4 conv, 2 strides, 32 ReLU	FC, 4x4x64 ReLU
4x4 conv, 2 strides, 32 ReLU	4x4 upconv, 2 strides, 64 ReLU
4x4 conv, 2 strides, 64 ReLU	4x4 upconv, 2 strides, 64 ReLU
4x4 conv, 2 strides, 64 ReLU	4x4 upconv, 2 strides, 64 ReLU
FC, 2 strides, 64 ReLU	4x4 upconv, 2 strides, num channels

Table 2: VAE-architecture used in this study for PBT-U-VAE (UDR) and PBT-S-VAE (MIG)

E.2 PBT hyperparameters

In our approach, unless defined otherwise, we implement the algorithm in the following way: A member \mathcal{M} consists of a β -TCVAE (Table 2) with parameters θ and optimizable hyperparameters $h = \{\text{learning rate}, \text{batch size}, \beta\}$. *step* is one epoch of SGD using Adam over the entire dataset. In *exploit*, the bottom 20% of the members according to their p each randomly copy the parameters θ of one of the top 20% of the members, *explore* perturbs the hyperparameters h by a factor randomly chosen from $\{0.5, 0.8, 1.2, 2\}$.

E.3 rPU-VAE Hyperparameters

Parameter	Value
$UDR_{threshold}$	0.1
$threshold_{UDR}$	0.005
$UDR_{patience}$	5 epochs
UDR num models	5
$dataset - size_{min}$	10
PBT population size	56
PBT parameters	$[\beta, \text{learning rate}, \text{batch size}]$
PBT perturbation factors	$[2, 1.2, 0.8, 0.5]$
PBT init batch sizes	$[8, 16, 32, 64, 128, 256, 512, 1024]$
PBT init learning rates	$(10^{-5} \dots 10^0, num = 30)$
PBT init β	$(1.5^1 \dots 1.5^{15}, num = 24)$
rPU-VAE supervised epochs	16
rPU-VAE supervised scoring function	MIG
VAE z dimension	10
number of leaf-runs	$[0, 1, 2, 3]$
$threshold_{z_{active}}$	0.5-1.0

Table 3: rPU-VAE Hyperparameters